Supplementary

Enhancing the oxygen reduction activity by constructing nanocluster-scaled Fe_2O_3/Cu interfaces

Qianjie Xie,[1#] Meiling Pan,[2#] Zheng Wang,*[3] Wenfang Si,[1] Ruiyi Zhang,[1] Yu Shu,[1] Guodong Sun,[c] Qun Jing,*[2] Yehua Shen,*[1] and Hiroshi Uyama[4]

[1]Key Laboratory of Synthetic and Natural Functional Molecule Chemistry of Ministry of Education, College of Chemistry and Materials Science, Northwest University, No. 1, Xuefu Road, 710127 Xi'an, Shaanxi, China.

[2]Xinjiang Key Laboratory of Solid State Physics and Devices, School of Physical Science and Technology, Xinjiang University, No. 777 Huarui Road, 830046 Urumqi, China.

[3]Xi'an Rare Metal Materials Research Institute Co., Ltd., No. 96 Weiyang Road, 710016 Xi'an, China.

[4]Department of Applied Chemistry, Graduate School of Engineering, Osaka University, Suita 565-0871, Japan.

[#]These authors contributed equally.

Corresponding author: Dr. Zheng Wang, zheng.wang@nwu.edu.cn; Prof. Qun Jing, qunjing@xju.edu.cn; Prof. Yehua Shen, yhshen@nwu.edu.cn.

Experiment

1. Electrocatalysts synthesis

Synthesis of $Zn_{2.7}Fe_{0.3}BTP_2$ and $Zn_{2.7}Fe_{0.2}Cu_{0.1}BTP_2$. $Zn_{2.7}Fe_{0.3}BTP_2$ was prepared according to the reported method with some modification.[1] 100 mg H_3BTP, 177.8 mg $Zn(OTf)_2$ and 13.8 mg $Fe(acac)_2$ for $Zn_{2.7}Fe_{0.3}BTP_2$ (or 9.2 mg $Fe(acac)_2$ together with 3.6 mg $Cu(OAc)_2 \cdot H_2O$ for $Zn_{2.7}Fe_{0.2}Cu_{0.1}BTP_2$) were dissolved in 7ml DMF in a round-bottomed flask and heated to 60 °C. 125 μL triethylamine was then added dropwisely to the solution under vigorous stirring. The mixture was refluxed at 162°C for 16 h. The brown precipitates was gathered by centrifuging, washed with DMF and methanol twice, and then dried under vacuum at 60 °C.

Synthesis of FeCu@NC. The as-synthesized $Zn_{2.7}Fe_{0.2}Cu_{0.1}BTP_2$ was blended well with melamine (1 : 3 by weight). Then the mixture was transferred into a tube furnace, heated to 900 °C at a heating rate of 5 °C min^{-1} and kept for 2 h under flowing Ar atmosphere to obtain FeCu@NC. The Fe@NC or Cu@NC was prepared by $Zn_{2.7}Fe_{0.3}BTP_2$ or $Zn_{2.7}Cu_{0.3}BTP_2$ with the same protocol, respectively.

2. Material characterization

Electrocatalyst characterization. The XRD patterns were collected on a Bruker D8 Aavance with Cu Kα radiation (λ = 1.5406 Å). The FT−IR spectra were carried out on a Bruker INVENIO R FT-IR spectrometric analyzer equipping ATR. Raman spectra were recorded on a LABRAM.HR dispersive Raman spectrometer with a excitation laser of 532 nm. XPS measurements were performed using a PHI 5000 Versaprode III spectrometer. The morphology and structure of the samples were investigated by SEM (HITACHI SU3500, Japan) and TEM (FEI Talos F200X, USA). Additionally, EDX elemental mappings of C, N, O, Fe and Cu were also measured. The SAC–TEM and EELS were recorded on a JEM-ARM200F. The N_2 adsorption/desorption isotherms were obtained using a Micromeritics 3flex instrument at 77 K. The pore size distributions of various carbonized products were

obtained by the Barrett−Joyner−Halenda (BJH) method. ICP−AES was done on an Agilent 7900 instrument.

ORR tests. All ORR measurements were carried out by using an electrochemical workstation (CHI 760E, CH Instruments, Inc., Shanghai) coupled with a rotating ring-disc electrode(RRDE) from Princeton Instruments (Model: 636A) in a typical three-electrode setup by employing Pt wire as counter electrode and Ag/AgCl as reference electrode. A rotating disk electrode (RDE) with a disk diameter of 5 mm covered by a thin film of the catalyst was used as the working electrode. To prepare the working electrode, 2 mg catalyst was ultrasonically dispersed in water/ethanol mixed solvent (1 mL, v/v = 1 : 9) containing 10 μL of 5 wt% Nafion solution. 25 μL of the catalyst ink was pipetted onto the RDE (loading amount: ~0.25 mg cm^{-2}). Cyclic voltammetry (CV) cycles experiments were carried out in the O_2-/N_2-saturated 0.1 M KOH solution with a scan rate of 50 mV s^{-1}. Linear-sweep voltammetry (LSV) measurements were performed in the O_2-saturated 0.1 M KOH solution with a scan rate of 5 mV s^{-1} at different rotating rate (400–2025 rpm). All potentials reported in this paper were converted to that of reversible hydrogen electrode (RHE).

The transferred electron numbers (n) was calculated by the Koutecký–Levich (K-L) equation expressed as follows:

$$\frac{1}{J}=\frac{1}{J_k}+\frac{1}{B\omega^{\frac{1}{2}}}$$

where J and J_k are the measured current density and the kinetic current density respectively, ω is the electrode rotating rate. B is determined from the Levich slope as given below:

$$B = 0.2\, n\, F\, C_0\, D_0^{\frac{2}{3}}\, v^{-\frac{1}{6}}$$

in which F is the Faraday constant (F = 96485 C mol^{-1}). C_0 is the concentration of O_2 in the 0.1 M KOH solution (C_0 = 1.2 × 10^{-6} mol cm^{-3}). D_0 is the diffusion coefficient of O_2 in electrolyte solution (D_0 = 1.9 × 10^{-5} cm^2 s^{-1}), and v is the kinematics viscosity of the

electrolyte (v = 0.01 cm^2 s^{-1}). The constant 0.2 is adopted when rotating speed is expressed in rpm.

The transferred electron numbers and H_2O_2 yield (H_2O_2%) were calculated from the RRDE measurement via the below equations:

$$H_2O_2\% = 200 \times \frac{I_r/N}{I_d + I_r/N}$$

$$n = 4 \times \frac{I_d}{I_d + I_r/N}$$

where I_d is the disk current, I_r is ring current and N is the current collection efficiency of the Pt ring with a value of 0.37.

Zn–air battery. Air cathodes were constructed by uniformly drop-casting FeCu@NC slurry over carbon paper followed drying for 60 °C for 4 h (loading mass: 1 mg cm^{-2}). For comparison, the same quantity Pt/C was also assembled in another battery. A polished zinc plate (thickness: 0.5 mm) was used as the anode and 6 M KOH solution containing 0.2 M $Zn(OAc)_2$ was used as the electrolyte. All the measurements were carried out at ambient condition. Cycling test was performed using recurrent galvanostatic pulses for 5 min of discharge followed by 5 min of charge at j = 5 mA cm^{-2}.

To assemble the solid-state sandwich-like layered Zn-air battery, a solid-state electrolyte was prepared by the following process.[2] First 7.2 mL acrylic acid monomers were mixed with 16.9 mL cellulose gel (1 wt%) slowly under vigorous stirring. Then the translucent solution was neutralized by 20 M sodium hydroxide aqueous solution. Afterwards, 4 mg N, N"-methylenebis-acrylamide and 110 mg ammonium persulfate were added and kept stirring for 0.5 h. The solution was degassed with N_2 for 10 min and maintained at 60 °C for 10 h to trigger the free-radical polymerization. After dried at 80 °C, the electrolyte was soaked in a mixed solution of 0.2 M zinc acetate and 6 M potassium hydroxide for 30 h to achieve the equilibrated state.

A flexible solid-sate ZAB was constructed by assembling a polished zinc foil (0.08 mm thickness), a piece of gel polymer electrolyte and an air electrode in a sandwich configuration. The air electrode was the carbon cloth loaded with the as-prepared catalyst (loading mass: 1 mg cm^{-2}). All measurements were conducted at room temperature. Similarly, the cycling test was performed using recurrent galvanostatic pulses for 5 min of discharge followed by 5 min of charge at j = 1 mA cm^{-2}.

3. DFT computational methods

Herein, spin-polarization DFT calculations were performed with the Vienna *ab initio* simulation package VASP. The exchange-correlation functional generalized[3] gradient approximation (GGA) of the Perdew, Burke, and Ernzerhof (PBE)[4] was used, and a plane wave basis set using the projector-augmented wave (PAW)[5] with 500 eV cutoff energy was employed. The Brillouin zone was sampled with 5 × 5 × 1 and 12 × 12 × 1 Monkhorst-Pack meshes for structure relaxation and electronic properties calculations, respectively. A 15 Å vacuum was added to avoid spurious interaction between layers in the Z direction. Convergence tolerance of electronic energy, maximum force was set as 1×10^{-5} eV and 0.02 eV $Å^{-1}$, respectively. Dispersion effects were augmented by Grimme's correction scheme of 2010 (DFT-D3).[6]

Monolayer graphene was used as a carbon carrier for Fe_2O_3@G (G = Graphene) electrocatalyst. The graphite Fe_2O_3 site was embedded in a 5 × 5 orthogonal graphene supercell containing 50 carbon sites, lattice parameter $a = b$ = 12.30 Å, and three-dimensional boundary condition was periodic. In addition, the Fe_2O_3/Cu@G system was constructed as follows: Firstly, six adjacent C atoms were removed from the original graphene plate to establish the carbon defect surface, and Fe_2O_3 clusters were embedded in the middle position of the carbon defect. Then, four N atoms were introduced to replace the C atoms directly connected to the two Fe atoms of the Fe_2O_3 clusters. Finally, just above the O atom in the

middle of Fe_2O_3 cluster was selected to connect with the Cu. In order to clarify the reason why Fe_2O_3 doping Cu can improve the catalytic performance of theoretical ORR, we selected three materials for comparison: Fe-N_x@G, Cu-N_x@G, Fe_2O_3@G, Fe_2O_3/Cu-N_4@G for DFT calculation. See Figure S17 for more details of models.

In alkaline electrolytes, the ORR on Fe_2O_3/Cu@G surfaces was considered to proceed along the 4e^- processes (overall process $O_2 + 2H_2O + 4\ e^- \rightarrow 4OH^-$), as below:

$$* + H_2O + O_2 + e^- \rightarrow HOO* + OH^- \quad (1a)$$

$$HOO* + e^- \rightarrow O* + OH^- \quad (1b)$$

$$O* + H_2O + e^- \rightarrow HO* + OH^- \quad (1c)$$

$$HO* + e^- \rightarrow OH^- + * \quad (1d)$$

where * stands for the adsorption site on the surfaces. To quantitatively assess the activity of the prepared Fe_2O_3/Cu@G catalysts, we calculated the binding energies of each intermediate following the approach of Nørskov *et al.* reported,[7-10]

$$\Delta E_{HOO*} = E_{HOO*} - E_* - \left[2E_{H_2O} - 3/2E_{H_2}\right] \quad (2)$$

$$\Delta E_{HO*} = E_{HO*} - E_* - \left[E_{H_2O} - 1/2E_{H_2}\right] \quad (3)$$

$$\Delta E_{O*} = E_{O*} - E_* - \left[E_{H_2O} - E_{H_2}\right] \quad (4)$$

where, for example, E_{*O} denoted the total energy of an oxygen atom adsorbed on the substrate obtained by the calculations, H_2O and H_2 in gas phases were used for references. The more positive of the binding energy, the weaker of the interaction between intermediates and the surfaces.

Then we converted the ground state energy into Gibbs free energy at standard state (298.15 K, 0.1 Mpa), and the solution pH of the adsorbates was also included,

$$\Delta G = \Delta E + \Delta ZPE - T\Delta S + \Delta G_U + \Delta G_{pH} \quad (5)$$

where, ΔE was the adsorption energy of each intermediate, ΔZPE and ΔS presented the differences of zero-point energy and entropy between the products and reactants, $\Delta G_U = -qU$,

where U is the electrode potential , $\Delta G_{pH} = k_B T \ln 10 \times (pH)$, k_B is the Boltzmann constant, in this work, pH = 14 was employed in the alkaline electrolyte.

The reference energy of O_2 and $OH^- - e^-$ were obtained from the following expressions,

$$G(O_2) = 2[G(H_2O) - G(H_2) - \triangle G_w] \quad (6)$$

$$G(OH^-) - G(e^-) = G(H_2O) - [G(H^+) + G(e^-)] = G(H_2O) - 1/2G(H_2) \quad (7)$$

where, ΔG_w = -2.46 eV was the experimental formation energy of water molecule. The detailed results can be seen in Table S3.

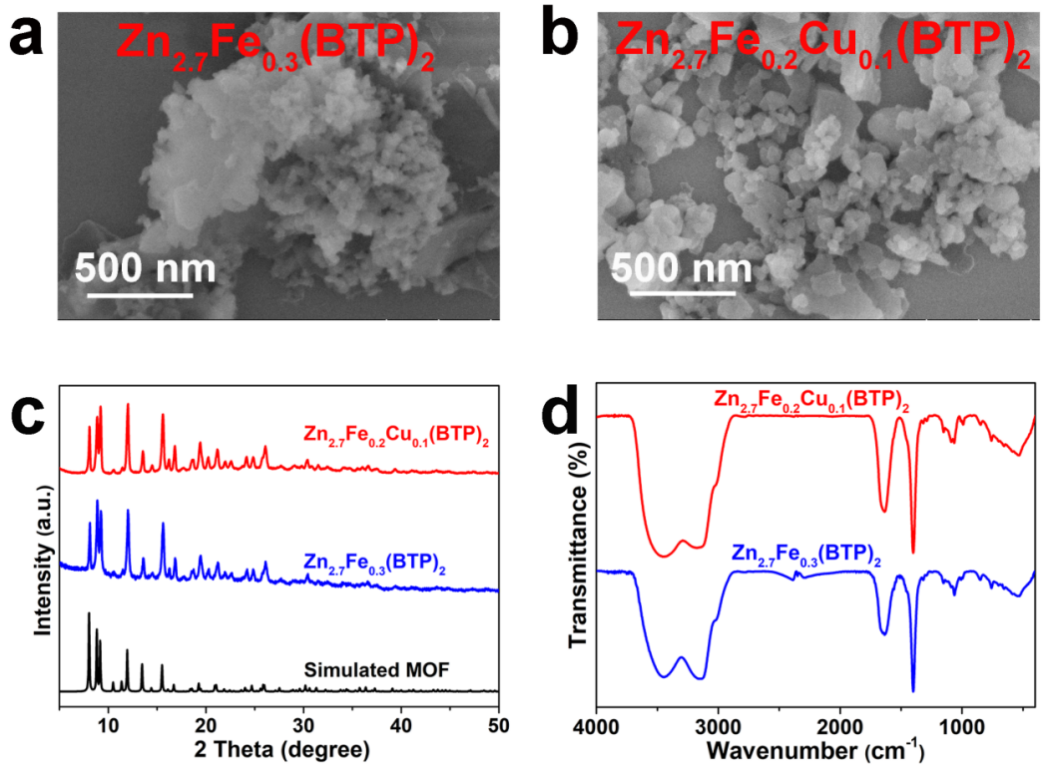

Figure S1. (a-b) The SEM images, (c) XRD patterns, (d) FT-IR spectra of $Zn_{2.7}Fe_{0.3}(BTP)_2$ and $Zn_{2.7}Fe_{0.2}Cu_{0.1}(BTP)_2$.

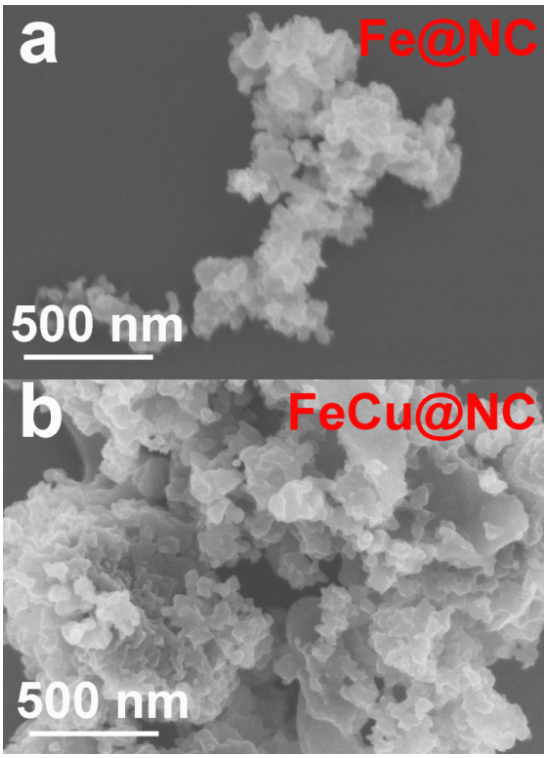

Figure S2. The scanning electron microscopy (SEM) images of (a) Fe@NC and (b) FeCu@NC.

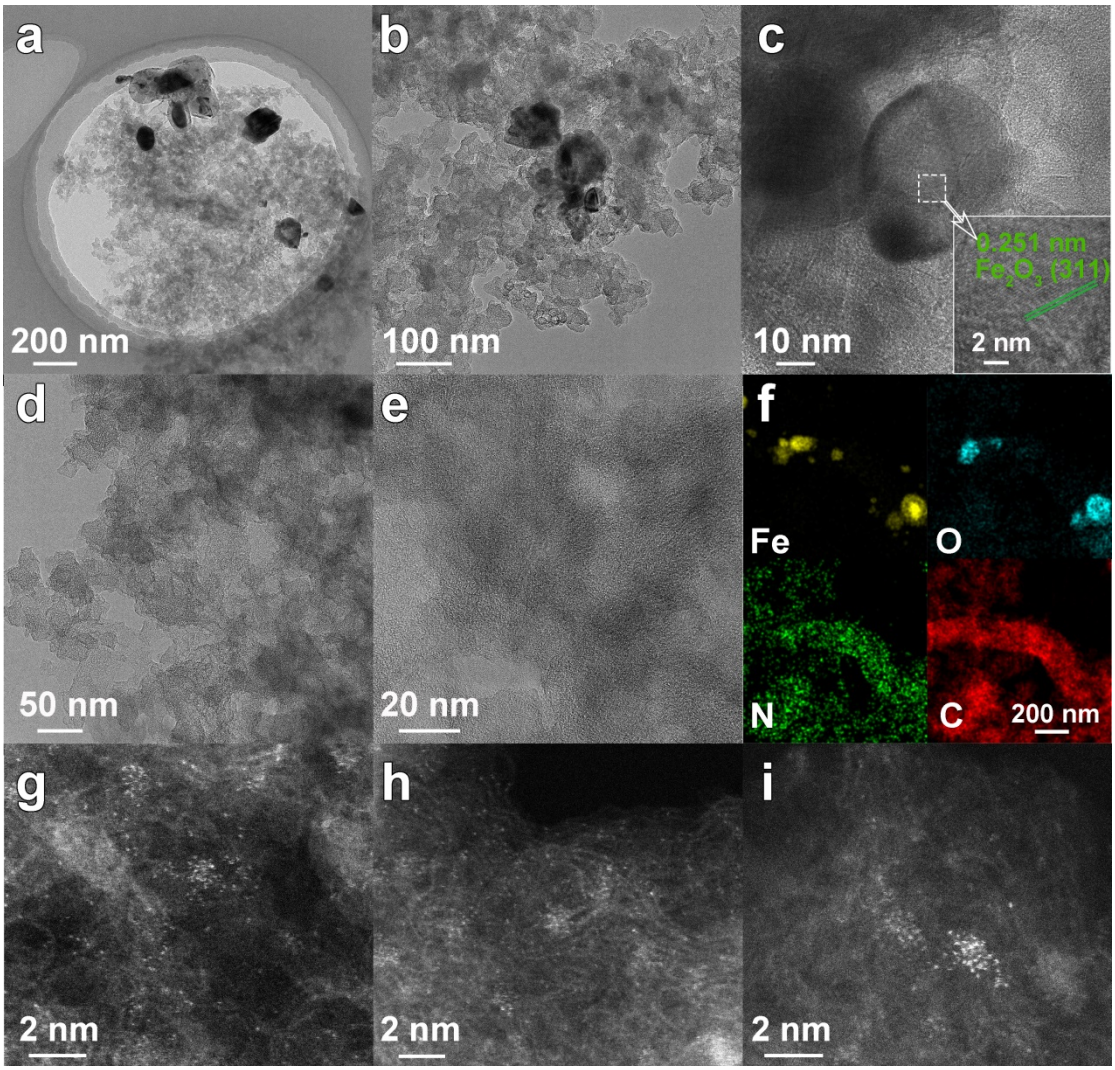

Figure S3. (a, b and d) The TEM images; (c, e) HRTEM images; (f) HAADF-STEM images and corresponding elemental mapping of Fe, O, N and C; (g-i) SAC-HAADF–STEM images of Fe@NC.

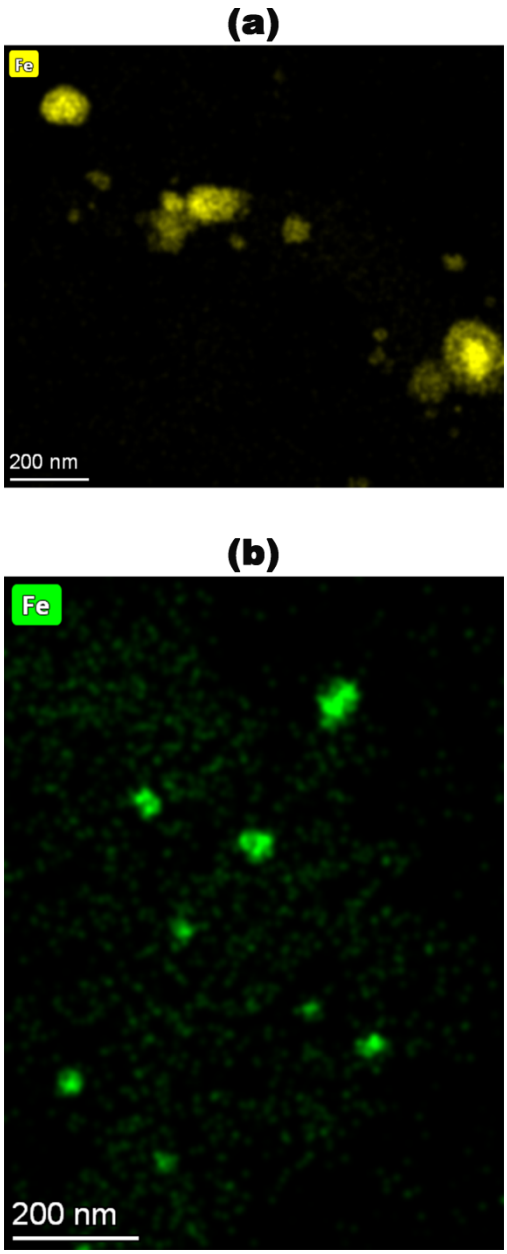

Figure S4. (a) The high-angle annular dark-field scanning TEM (HAADF-STEM) of Fe of Fe@NC, (b) of FeCu@NC.

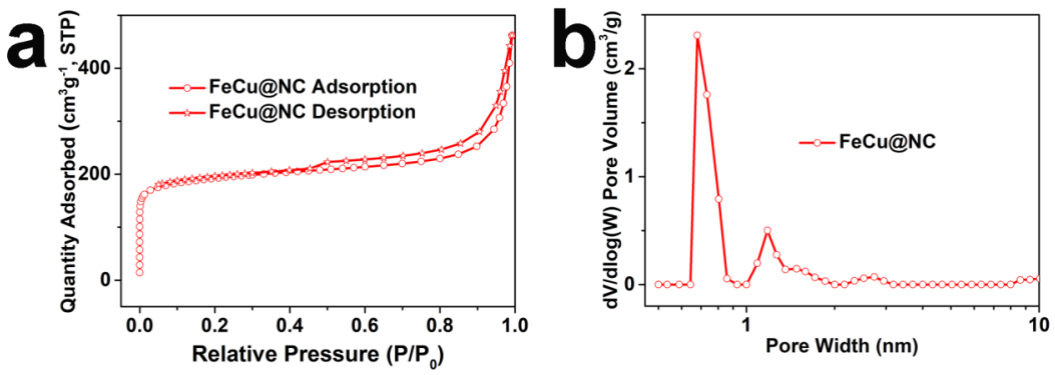

Figure S5. (a) The N_2 sorption isotherms and (b) the pore size distributions of FeCu@NC.

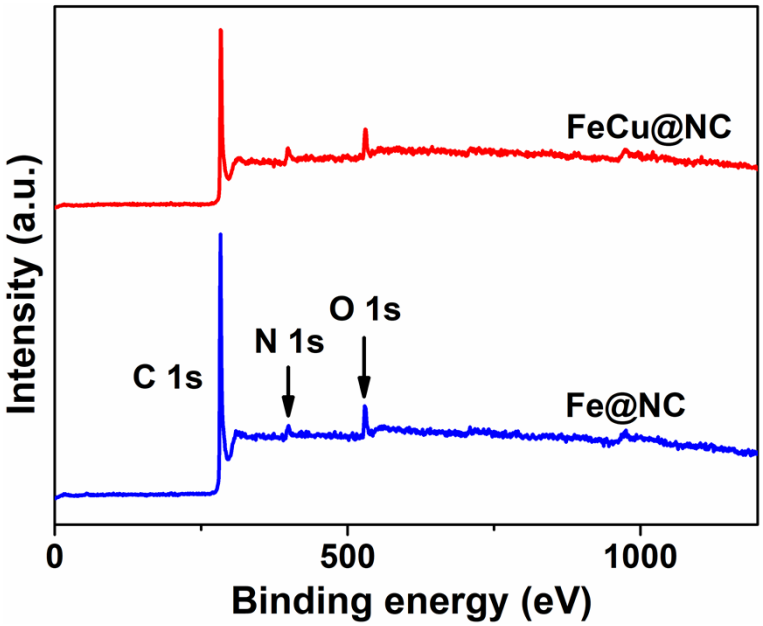

Figure S6. The full X-ray photoelectron spectroscopy (XPS) spectra of (a) FeCu@NC and (b) Fe@NC.

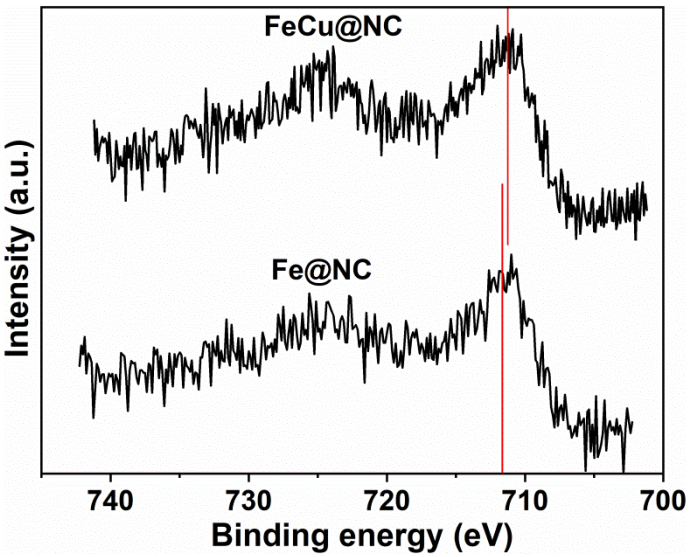

Figure S7. The original Fe 2p spectra of FeCu@NC and Fe@NC.

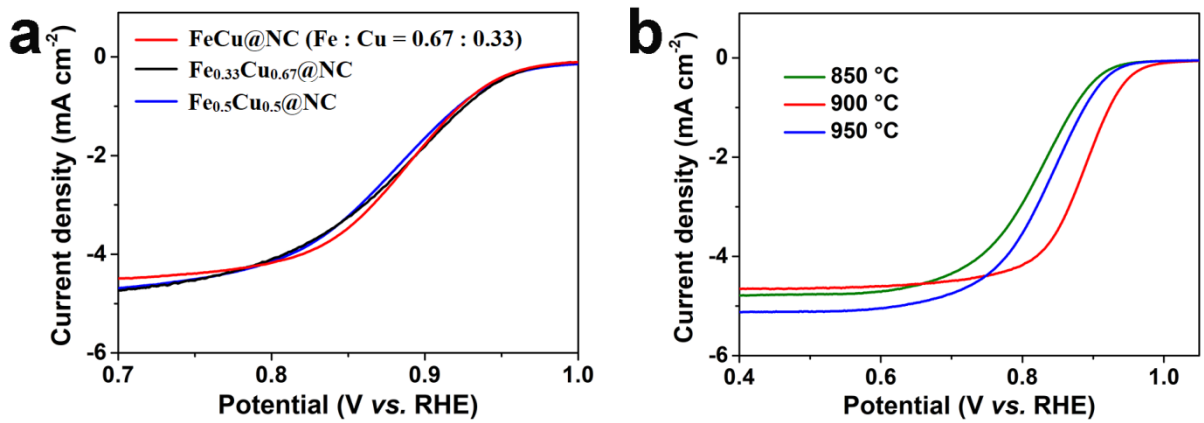

Figure S8. The catalysts derived (a) with different Fe/Cu ratio (0.33/0.67, 0.5/0.5 and 0.67/0.33) and (b) under different pyrolysis temperature (850 °C, 900 °C and 950°C).

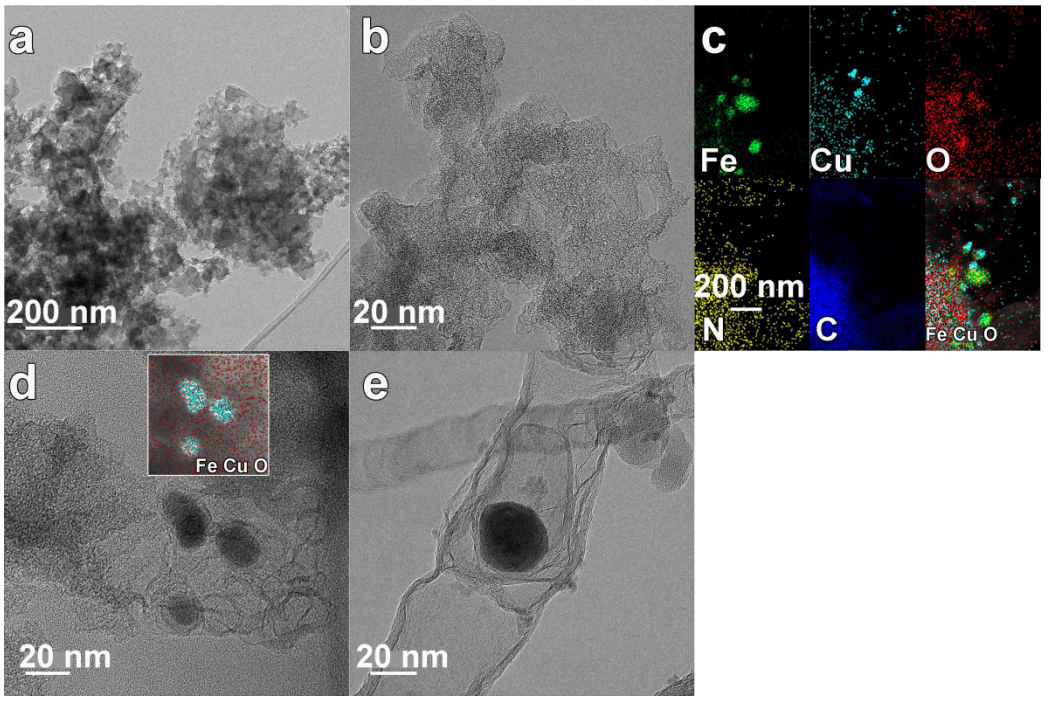

Figure S9. TEM images of FeCu@NC after acid treatment. Viewing from a–c, the nanoparticles were also observed as well as the carbon matrix was corroded with more pores. Closer inspection in d revealed that part of the nanopartilces were etched with carbon matrix left only. As shown in e, it is easy to recognize that the heterojunction was destroyed with half space of the carbon matrix inclued empty.

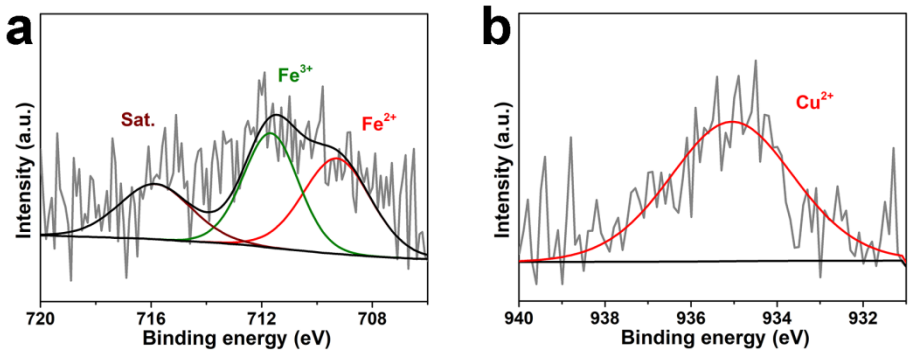

Figure S10. (a) Fe 2p and (b) Cu 2p XPS spectra of FeCu@NC after acid treatment. Comparing with the fresh catalyst, the relative intensity of Fe^{3+} $2p_{3/2}$ (vs Fe^{2+} $2p_{3/2}$) of FeCu@NC decreased after acid etching, confirming that the part of the Fe nanoparticles and nanoclusters were diminished (Figure S10, SI). While Cu^0 $2p_{3/2}$ peaks were disappeared, which indicated that the Cu nanoparticles/nanoclusters located the surfaces of FeCu@NC were removed after acid treatment.

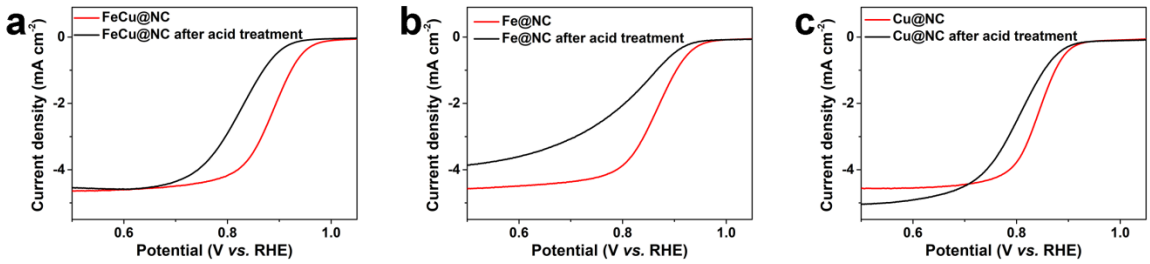

Figure S11. The comparison of ORR polarization of (a) FeCu@NC, (b)Fe@NC and (c) Cu@NC before and after acid treatment in an O_2-saturated 0.1 M of KOH solution at 5 mV s^{-1} with 1600 rpm. It is apparent that the ORR activity of studied catalysts was obviously decreased after acid treatment, because their structures were destroyed.

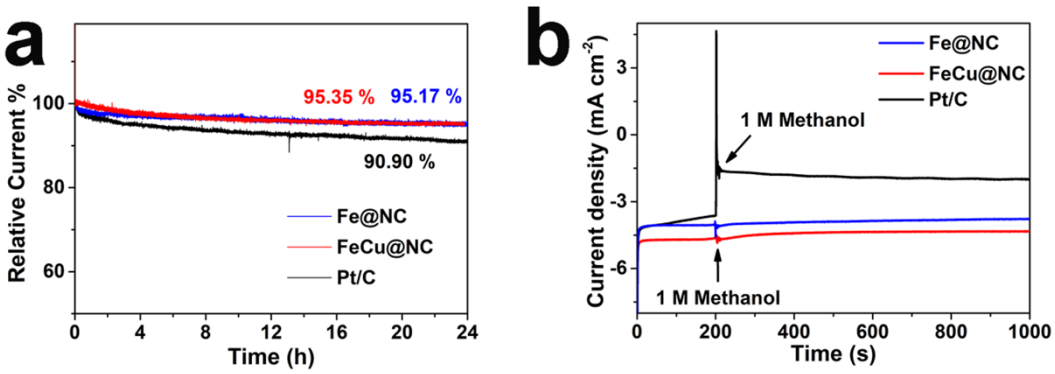

Figure S12. (a) Amperometric i-t curves at applied potential of 0.5 V, (b) i–t responses at 0.5 V and 1600 rpm by adding 1.0 M methanol at around 200 s of Fe@NC, FeCu@NC and 20 wt% Pt/C.

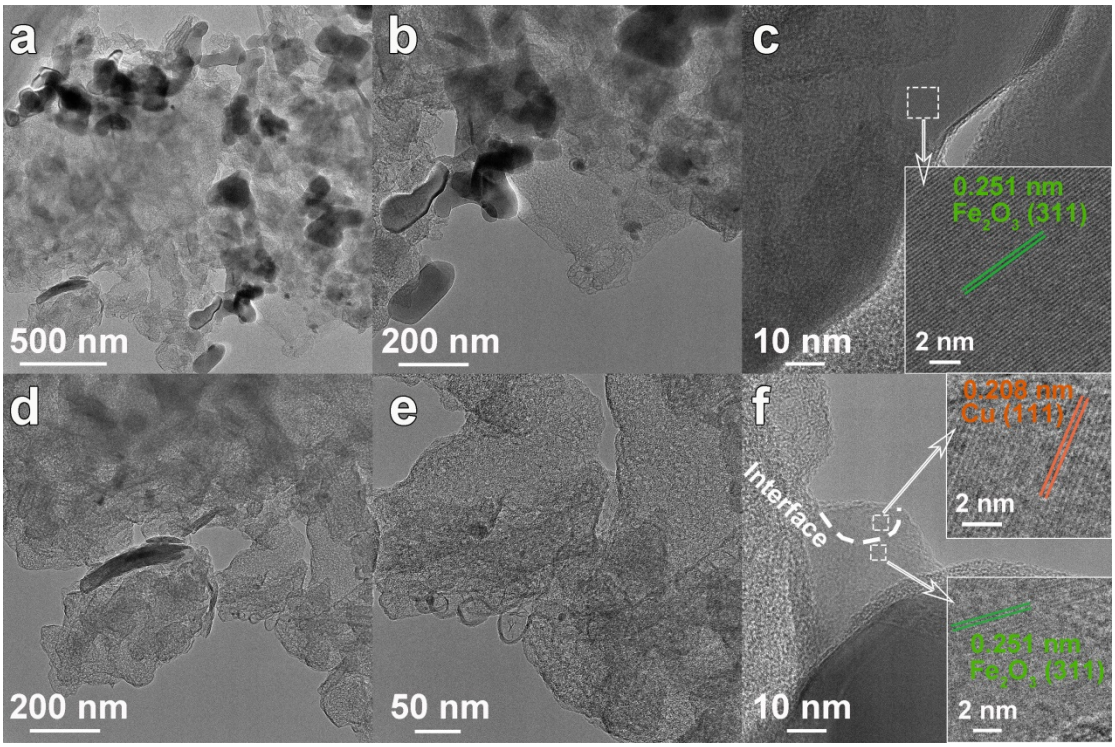

Figure S13. (a, b, d and e) The TEM images; (c and f) HRTEM images of FeCu@NC after stability test.

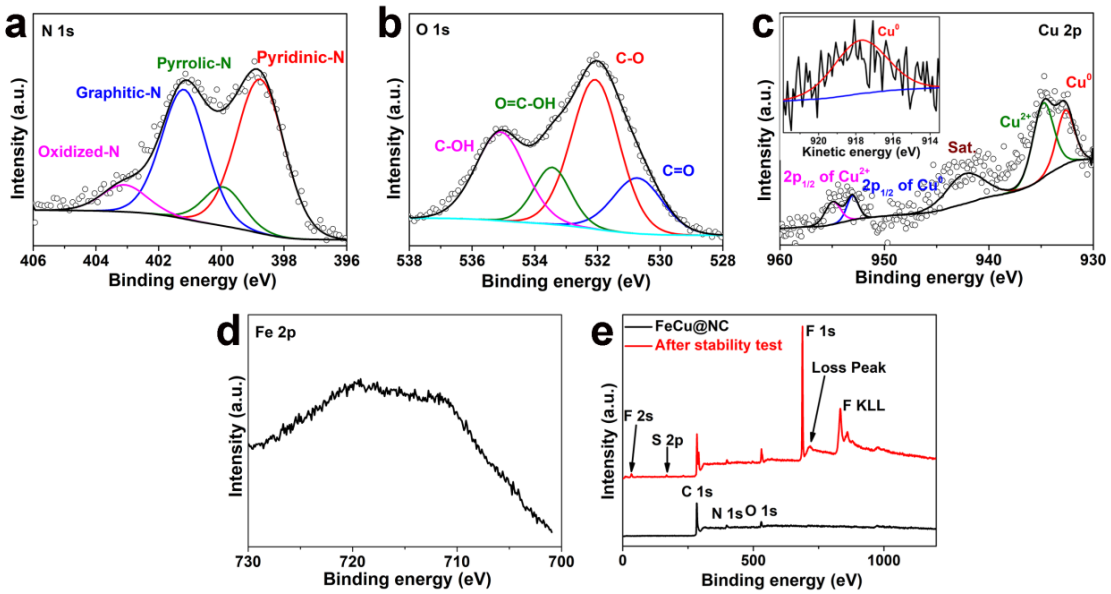

Figure S14. The (a) N 1s, (b) O1s, (c) Cu 2p (inset: Cu LMM Auger spectrum), (d) Fe 2p and (e) full XPS spectra of FeCu@NC after stability test.

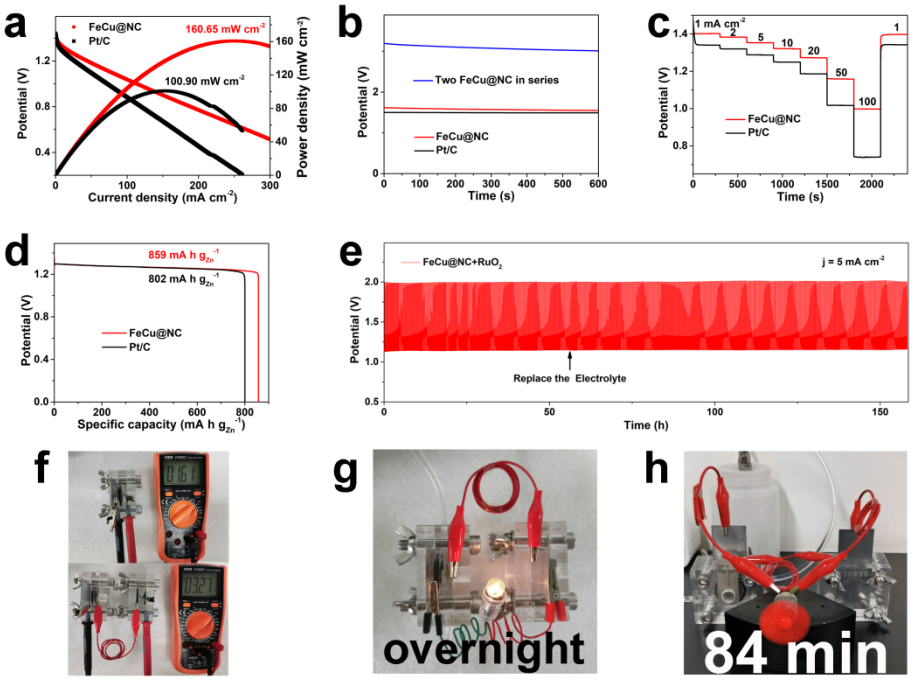

Figure S15. ZAB performances with FeCu@NC catalyst as the air cathode in comparison with the Pt/C catalysts. (a) Discharge polarization curves and the corresponding power density curves of FeCu@NC and Pt/C assembled batteries; (b) OCV of FeCu@NC and Pt/C batteries; (c) rate performance of FeCu@NC bettery at a current density of 1, 2, 5, 10, 20, 50, 100 and 1 mA cm^{-2}; (d) specific capacities of FeCu@NC and Pt/C batteries; (e) cycling performance of rechargeable ZABs with the FeCu@NC|RuO_2 cathodes at 5 mA cm^{-2}; (f) photograph of a liquid battery or two batteries in series with an open-circuit voltage of 1.61 V or 3.27 V; photograph of (g) a lamp and (h) a motor powered by two ZABs in series.

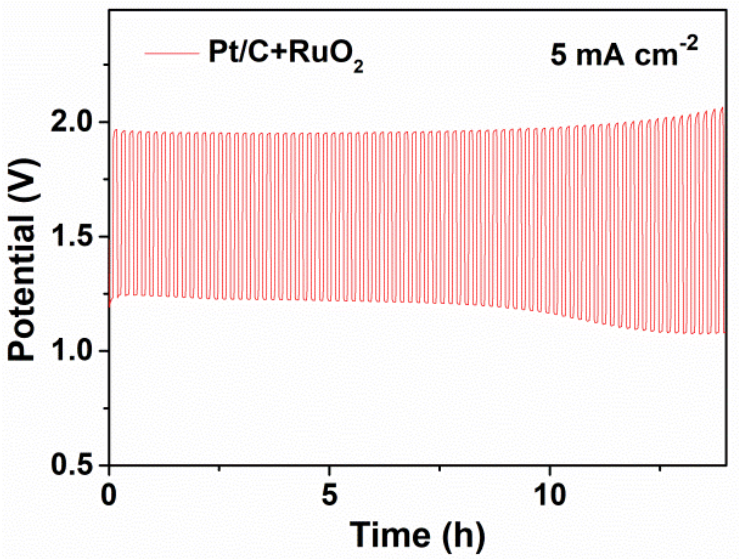

Figure S16. Cycling performance of Pt/C|RuO_2 based ZAB at 5 mA cm^{-2}.

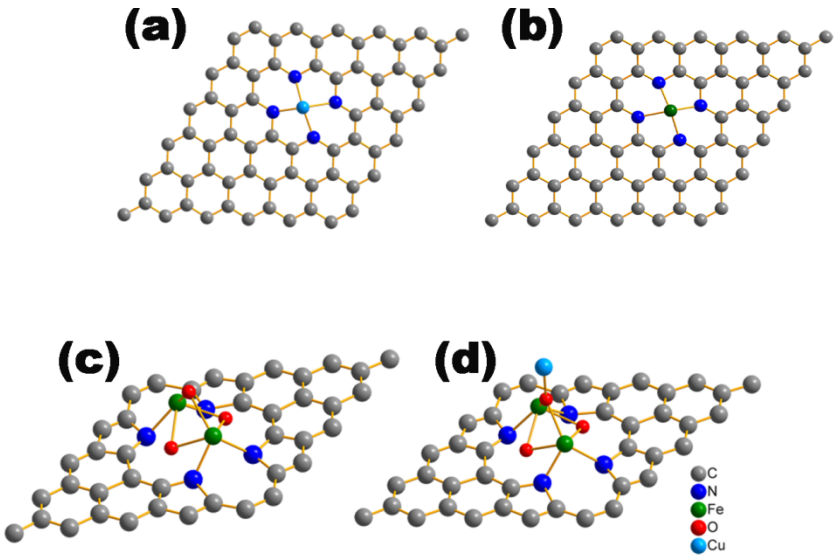

Figure S17. The models of (a) Fe-N_x@G, (b) Cu-N_x@G, (c) Fe_2O_3@G, and (d) Fe_2O_3/Cu@G. The metallic species were doped in 5 × 5 graphene via four N atoms.

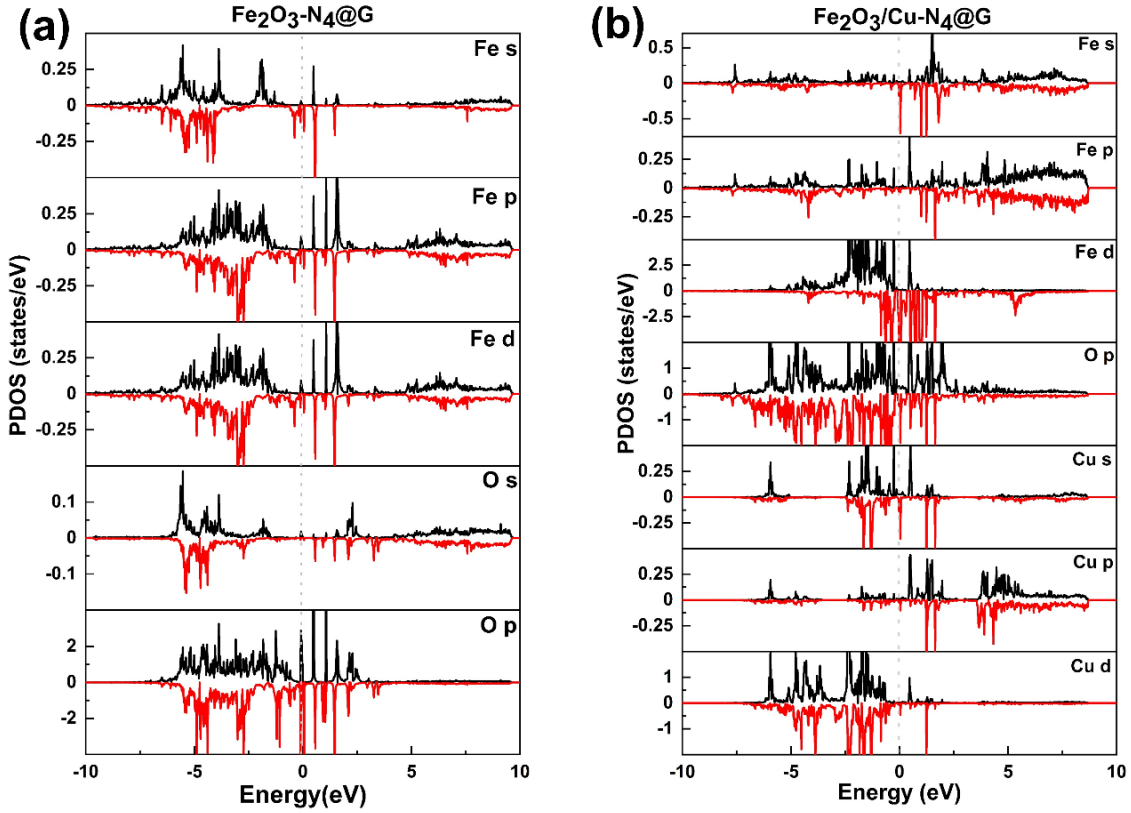

Figure S18. The partial densities of states (PDOS) of (a) Fe_2O_3-N_4@G and (b) Fe_2O_3/Cu-N_4@G.

Table S1. The relative content of total N, pyridinic N, pyrrolic N and graphitic N.

Content	Total N	Pyridinic N	Pyrrolic N	Graphitic N
Fe@NC	3.10%	29.75%	11.53%	47.66%
FeCu@NC	6.63%	46.26%	10.50%	36.62%

Table S2. Comparison of FeCu@NC based flexible solid-state ZAB and the reported catalysts.

Catalyst	OCV (V)	power density (mW cm^{-2})	power density of noble metal catalyst (mW cm^{-2})	Durability	Ref.
FeCu@NC	1.641	118.5	69.45	30 h (180 cycles)	This work
Ni/CNF-750	1.38	56.8	/	16 000 s	[11]
Co/CoO@NS	1.43	82.7	80.7	143 h (858 cycles)	[12]
CN@NC−2−800	1.44	/	/	12 h (72 cycles)	[13]
Fe_1/d-CN	1.50	78.0	22.0	20 h	[14]
FeCo/Se-CNT	1.405	37.5	/	20 h	[15]
$NiCo_2O_4$/MXene	1.40	55.1	/	100 cycles	[16]
Ni_3Fe/NPG-1	1.45	50.0	/	150 cycles	[17]
FeP/Fe_2O_3@NPCA	1.42	40.8	/	500 min	[18]
NdDCF-OIM/Co-800	1.346	84	/	165 cycles (55 h)	[19]
$(Fe,Co,Ni)_9S_8$/NSCFs	1.435	80.1	/	140 cycles	[20]
P-CoO@PWC-2	1.47	73	/	67 h (200 cycles)	[21]
Fe-N-C on 2D porous carbon	1.48	210.5	/	110 h	[2]
NOC-1000-1	1.48	100.92	72.18	30 h/180 cycles	[22]
Fe-N-C-700	1.424	70	/	/	[23]
Co-N-900	1.32	131.81	/	16.7 h/100 cycles	[24]
Fe-N-C	1.4	55.86	40.59	250 min	[25]

Table S3. The calculated adsorption energies ΔE (eV), zero point energies ZPE, entropy TS and Gibbs free energy changes ΔG (eV) of different reaction intermediates on grephene monolayers.

Samples	*OO intermediate			*OOH intermediate			*O intermediate			*OH intermediate		
	ΔE_{*OO}	ZPE	TS	ΔE_{*OOH}	ZPE	TS	ΔE_{*O}	ZPE	TS	ΔE_{*OH}	ZPE	TS
Pt/C	3.528	0.121	0.219	2.565	0.431	0.213	1.042	0.056	0.105	0.440	0.340	0.127
CuN_4@G	10.075	0.101	0.222	9.764	0.410	0.258	9.403	0.034	0.110	6.823	0.312	0.173
Fe_2O_3-N_4@G	5.758	0.164	0.092	4.573	0.433	0.201	3.898	0.086	0.038	1.696	0.337	0.121
Fe_2O_3/Cu-N_4@G	2.179	0.131	0.161	-0.339	0.428	0.204	0.846	0.072	0.068	-1.996	0.334	0.120

Reference:

1. V. Colombo, S. Galli, H. J. Choi, G. D. Han, A. Maspero, G. Palmisano, N. Masciocchi and J. R. Long, *Chem. Sci.*, 2011, **2**, 1311.
2. L. Ma, S. Chen, D. Wang, Q. Yang, F. Mo, G. Liang, N. Li, H. Zhang, J. A. Zapien and C. Zhi, *Adv. Energy Mater.*, 2019, **9**, 1803046.
3. J. P. Perdew and Y. Wang, *Phys. Rev. B*, 1992, **45**, 13244.
4. J. P. Perdew, K. Burke and M. Ernzerhof, *Phys. Rev. Lett.*, 1996, **77**, 3865.
5. G. Kresse and D. Joubert, *Phys. Rev. B*, 1999, **59**, 1758.
6. S. Grimme, *J. Comput. Chem.*, 2006, **27**, 1787.
7. T. Bligaard, J. K. Nørskov, S. Dahl, J. Matthiesen, C. H. Christensen and J. Sehested, *J. Catal.*, 2004, **224**, 206.
8. J. K. Nørskov, J. Rossmeisl, A. Logadottir, L. Lindqvist, J. R. Kitchin, T. Bligaard and H. Jonsson, *J. Phys. Chem. B*, 2004, **108**, 17886.
9. J. Greeley, I. Stephens, A. Bondarenko, T. P. Johansson, H. A. Hansen, T. Jaramillo, J. Rossmeisl, I. Chorkendorff and J. K. Nørskov, *Nat. Chem.*, 2009, **1**, 552.
10. G. Tritsaris, J. Greeley, J. Rossmeisl and J. K. Nørskov, *Catal. Lett.*, 2011, **141**, 909.
11. G. Liu, X. Xia, C. Zhao, X. Zhang and W. Zhang, *J. Colloid Interface Sci.*, 2021, **588**, 627.
12. D. Zhou, H. Fu, J. Long, K. Shen and X. Gou, *J. Energy Chem.*, 2022, **64**, 385.
13. Z. Zhu, Q. Xu, Z. Ni, K. Luo, Y. Liu and D. Yuan, *ACS Sustain. Chem. Eng.*, 2021, **9**, 13491.
14. M. Zhao, H. Liu, H. Zhang, W. Chen, H. Sun, Z. Wang, B. Zhang, L. Song, Y. Yang, C. Ma, Y. Han and W. Huang, *Energy Environ. Sci.*, 2021, **14**, 6455.
15. H. Zhang, M. Zhao, H. Liu, S. Shi, Z. Wang, B. Zhang, L. Song, J. Shang, Y. Yang, C. Ma, L. Zheng, Y. Han and W. Huang, *Nano Lett.*, 2021, **21**, 2255.
16. H. Lei, S. Tan, L. Ma, Y. Liu, Y. Liang, M. S. Javed, Z. Wang, Z. Zhu and W. Mai, *ACS Appl. Mater. Interfaces*, 2020, **12**, 44639.
17. X. Hao, Z. Jiang, X. Tian, C. Song, S. Chen, X. Hao and Z.-J. Jiang, *ACS Appl. Energy Mater.*, 2020, **3**, 12148.
18. K. Wu, L. Zhang, Y. Yuan, L. Zhong, Z. Chen, X. Chi, H. Lu, Z. Chen, R. Zou, T. Li, C. Jiang, Y. Chen, X. Peng and J. Lu, *Adv. Mater.*, 2020, **32**, e2002292.
19. J. Zhao, H. Hu, W. Fang, Z. Bai, W. Zhang and M. Wu, *J. Mater. Chem. A*, 2021, **9**, 5097.
20. T. Jiang, P. Dai, W. Zhang and M. Wu, *Electrochim. Acta*, 2021, **373**, 137903.
21. H. Liu, Y. Liu, S. Mehdi, X. Wu, T. Liu, B. Zhou, P. Zhang, J. Jiang and B. Li, *Adv. Sci.*, 2021, **8**, 2101314.
22. Q. Xie, W. Si, Y. Shen, Z. Wang and H. Uyama, *Nanoscale*, 2021, **13**, 16296.
23. T. Chen, J. Wu, C. Zhu, Z. Liu, W. Zhou, C. Zhu, C. Guan and G. Fang, *Chem. Eng. J.*, 2021, **405**, 125956.
24. D. Su, X. Wang, Y. Liu, S. Xu, S. Fang, S. Cao and Y. Xiao, *J. Alloys Compd.*, 2022, **896**, 162604.
25. W. Zhai, S. Huang, C. Lu, X. Tang, L. Li, B. Huang, T. Hu, K. Yuan, X. Zhuang and Y. Chen, *Small*, 2022, **18**, e2107225.